Biophysical Journal
Article

Biophysical Society

Non-Langmuir Kinetics of DNA Surface Hybridization

Luka Vanjur,[1] Thomas Carzaniga,[1] Luca Casiraghi,[1] Marcella Chiari,[2] Giuliano Zanchetta,[1] and Marco Buscaglia[1,*]

[1]Dipartimento di Biotecnologie Mediche e Medicina Traslazionale, Università degli Studi di Milano, Segrate, Italy and [2]Consiglio Nazionale delle Ricerche, Istituto di Chimica del Riconoscimento Molecolare, Milano, Italy

ABSTRACT Hybridization of complementary single strands of DNA represents a very effective natural molecular recognition process widely exploited for diagnostic, biotechnology, and nanotechnology applications. A common approach relies on the immobilization on a surface of single-stranded DNA probes that bind complementary targets in solution. However, despite the deep knowledge on DNA interactions in bulk solution, the modeling of the same interactions on a surface are still challenging and perceived as strongly system dependent. Here, we show that a two-dimensional analysis of the kinetics of hybridization, performed at different target concentrations and probe surface densities by a label-free optical biosensor, reveals peculiar features inconsistent with an ideal Langmuir-like behavior. We propose a simple non-Langmuir kinetic model accounting for an enhanced electrostatic repulsion originating from the surface immobilization of nucleic acids and for steric hindrance close to full hybridization of the surface probes. The analysis of the kinetic data by the model enables quantifying the repulsive potential at the surface, as well as retrieving the kinetic parameters of isolated probes. We show that the strength and the kinetics of hybridization at large probe density can be improved by a three-dimensional immobilization strategy of probe strands with a double-stranded linker.

SIGNIFICANCE Hybridization of nucleic acids strands with complementary sequences is a fundamental biological process and is also widely exploited for diagnostic purposes. Despite the availability of effective models for the equilibrium strength of freely diffusing strands, a general predictive model for surface hybridization is still missing. Moreover, the kinetics of hybridization is not fully understood either in solution or on a surface. In this work, we show that the analysis of the kinetics of hybridization on a surface reveals and enables to quantify two main additional contributions: electrostatic repulsion and steric hindrance. These are general effects expected to occur not only on a surface but in any condition with large density of nucleic acids comparable to that of the cellular nucleus.

INTRODUCTION

The formation of double-stranded DNA (dsDNA) from two complementary strands, called hybridization, is a fundamental process underlying DNA microarray technology (1), as well as the rapidly expanding field of DNA nanotechnology (2). DNA microarrays (DNA chips) have proven to be a powerful tool in many biomedical applications, from detecting single-nucleotide polymorphisms to gene expression analysis (3). DNA chips are comprised of single-stranded DNA (ssDNA) immobilized on a surface and acting as probes for complementary ssDNA in solution. Current research efforts in this field focus on two main goals: the development of novel physicochemical methods to improve the transduction of the sensor signal and the design of molecular mechanisms to enhance the sensitivity and specificity of probe-target recognition (4,5). In particular, DNA nanotechnology offers the opportunity to control the structure and function of complex supramolecular systems and enables the design of programmable molecular machines (6).

A current limitation on the integration of DNA nanomachines on a biosensor surface is that the hybridization with a complementary strand immobilized on a surface generally displays a reduced affinity in comparison with the case in which both strands are freely diffusing in solution (7,8). Interestingly, such difference between bulk and surface interactions is typically not observed for

Submitted February 27, 2020, and accepted for publication July 21, 2020.

*Correspondence: marco.buscaglia@unimi.it

Editor: Susan Schroeder.

https://doi.org/10.1016/j.bpj.2020.07.016

protein-protein binding (e.g., antibody-antigen) and appears to be a characteristic of the nucleic acid (NA) recognition process. Different possible causes of this phenomenon have been proposed (9–11). More generally, the electrostatic repulsion plays an important role in the decreased hybridization strength on a surface. Indeed, ssDNA is a polyelectrolyte in which each repeating unit bears one negative charge. The accumulation of ssDNA probes on a surface has been reported to induce an effective repulsive potential on freely diffusing complementary strands (12,13), which shifts the equilibrium of hybridization in comparison to the same interaction in solution.

Similar to equilibrium parameters, the kinetics of surface hybridization also significantly differs from the same process in the bulk (14–17). Despite being fundamental to understanding the origin of the equilibrium features, the kinetics of surface-bound DNA hybridization is still poorly understood (18). A direct access to real-time binding curves without interference from labeling moieties is provided by label-free biosensors. Since the first studies performed by surface plasmon resonance, it has been shown that the real-time binding curves for DNA hybridization can depend on a number of factors, including the probe surface density, the probe distance from the surface, and the presence of mismatches, and it can display nonexponential behavior, in contrast with a simple Langmuir interaction model describing independent binding events (14,19,20). However, a general molecular interaction model to account for the kinetic curves for DNA hybridization on a surface is still missing. Indeed, the kinetics of hybridization is not fully understood even in the more standard case in which both complementary strands are freely diffusing in solution (18,21). In this context, label-free biosensors not only represent a promising application field in which to exploit DNA nanotechnology, but they also provide an effective analytical tool to characterize DNA hybridization at molecular level. Several label-free biosensors have been exploited for sequence detection or quantification (22–26). Among these, reflective phantom interface (RPI) measures the increase of intensity of light reflected by an interface with very low reflectivity upon binding of molecular targets on surface-immobilized probes. RPI has been demonstrated as a sensitive tool to characterize the kinetic and equilibrium parameters of biomolecular recognition process (27,28) and, in particular, of fully or partially complementary oligonucleotides (11).

Here, we show that the DNA hybridization kinetic curves acquired by label-free optical signals display marked deviations from a Langmuir behavior in a wide range of conditions. We explored different surface densities of complementary probes immobilized with or without a DNA linker, either ss or ds. We studied the hybridization at different concentrations of target strand in solution and ionic strengths. We found that both the equilibrium behavior and the kinetics of hybridization show discrepancies from an ideal Langmuir interaction in all explored conditions. The results support the primary effect of electrostatic repulsion originating in proximity of the surface because of NA accumulation. Moreover, close to saturation of the surface probes by complementary targets, we observed a marked decrease of the apparent kinetic constant for hybridization as a consequence of surface crowding. The measured reduction of hybridization affinity at large local NA concentrations strongly affects the results of DNA or RNA microarrays and biosensors and can play a biological role in the cellular environments rich in DNA, such as the nucleus. In general, the enhanced repulsion observed for the hybridization at large DNA local density could contribute to keeping a large specificity of pairing even in a DNA-crowded environment.

MATERIALS AND METHODS

DNA strands and reagents

We studied the kinetics of hybridization of a 12-mer model sequence with different surface-immobilized complementary probes. As schematically shown in Fig. 1, the simplest interaction with a 12-mer probe (no linker) was compared to that measured with probes having an additional ss-linker or ds-linker. The NA sequences used in this work are reported in Table 1. Probe strands p1 and p2 were immobilized on the RPI sensing surface, and t1 was used as a complementary target strand in solution. Strand cp2 was optionally used to make a dsDNA spacer at the base of p2. ssDNA

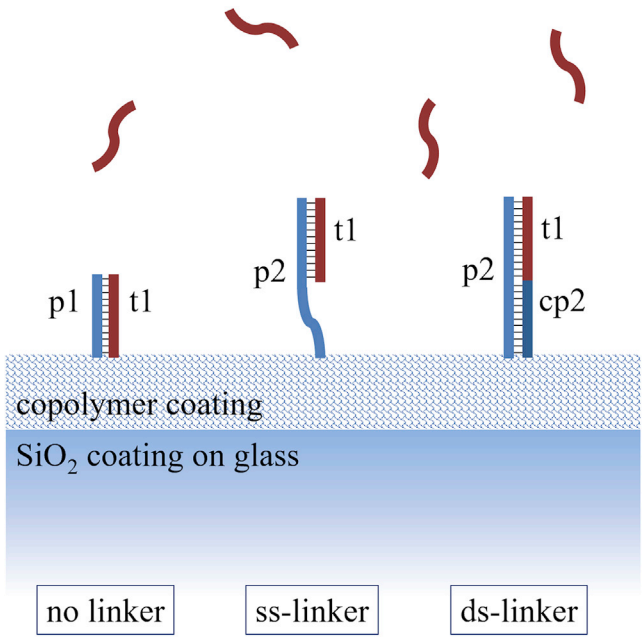

FIGURE 1 Schematics of surface probe types. The 12-mer target strand t1 (*dark red*) binds to a complementary probe strand (*blue*) immobilized on the RPI sensing surface by a 3D copolymer coating. Three types of DNA probes were investigated: a complementary 12-mer strand (p1, no linker scheme) and longer probes formed by an ss strand (p2, ss-linker) or a ds strand (p2 + cp2, ds-linker) terminated with the complementary sequence. To see this figure in color, go online.

TABLE 1 DNA Sequences

Name	Bases	Sequence
p1	12	/5AmMC6/AGG TAA AAG TGA
p2	23	/5AmMC6/GCC CAC CTA TAA GGT AAA AGT GA
cp2	11	TAT AGG TGG GC
t1	12	TCA CTT TTA CCT

were purchased from Integrated DNA Technologies (Leuven, Belgium) with high-quality Ultramer synthesis. Strands p1 and p2 were amine modified at the C6 carbon of 5′ terminal (5AmMC6 in Table 1). The surface immobilization of amine-terminated ssDNA was achieved by coating the RPI sensing chip with MCP2 or MCP4 copolymers from Lucidant Polymers (Sunnyvale, CA). They are copolymers of dimethylacrylamide, N-acryloyloxysuccinimide, and 3-(trimethoxysilyl)propyl methacrylate, and they differ only in the comonomer molar ratio: 97:2:1 in MCP2 and 89:10:1 in MCP4. The fraction of amine-reactive sites of MCP4 is five times larger than that of MCP2. All buffers and reagents were purchased from Sigma-Aldrich (St. Louis, MO) and prepared according to common protocols using Milli-Q pure water.

RPI sensor preparation and measurement

DNA probe strands were covalently immobilized on the surface of RPI sensing chips in spots with 150–200 μm diameter, following the procedure described in (28). Briefly, 8 × 12 mm wedge-like chips of F2 optical glass (Schott, Mainz, Germany) coated with an antireflection layer of SiO_2, were plasma cleaned and dip coated with MCP2 or MCP4 copolymer (29). Droplets of spotting buffer (Na_2HPO_4 (pH 8.5) 150 mM) containing amine-terminated DNA probes at concentrations from 1 up to 30 μM were deposited on the chip surface by an automated noncontact dispensing system (sciFLEXARRAYER S5; Scienion AG, Berlin, Germany). After overnight incubation, the chip surface was rinsed with blocking buffer (Tris-HCl (pH 8) 10 mM, NaCl 150 mM, ethanolamine 50 mM) and distilled water and then dried. The sensor cartridges were prepared by gluing the glass chips on the inner wall of 1 cm plastic cuvettes. The cartridges were stored at 4°C before use. Target ssDNA strand t1 and strand cp2 were suspended before use in measuring buffer (10 mM Tris-HCl, 0.02% NaN_3 (pH 8.0) + NaCl at different concentrations depending on the measurement).

The RPI measurements were performed by using the apparatus and the analysis algorithm described in (28). The sensor cartridges were filled with 1.3 mL of measuring buffer. The ionic strength was adjusted by adding NaCl from 75 up to 220 mM. In the experiments performed with the ds-linker probe, the strand cp2 was added at a concentration of 1.5 μM at least 1 h before the measurement to keep the fraction of p2 probes hybridized with the cp2 strand as large as 99% or more during the measurement. The cartridges were kept at 23°C during the measurement through a thermalized holder, and rapid mixing of the solution was provided by a magnetic stirring bar. Sample spikes of target ssDNA were performed by adding 50 μL of measuring buffer containing different amounts of target molecules to a final concentration in the cartridge from 0.5 nM up to ~1.5 μM. Time sequences of RPI images of the spotted surface were analyzed by a custom MATLAB program (The MathWorks, Natick, MA) to obtain the brightness of each spot as a function of time t and convert it into the total mass surface density of molecules $\sigma(t)$ (Supporting Materials and Methods) and into the mass surface density of the target molecules $\sigma_t(t) = \sigma(t) - \sigma_p(t)$, where $\sigma_p(t)$ is the mass surface density of immobilized probe molecules measured before the addition of the target ssDNA in solution.

The analysis of the hybridization curves was performed on $\sigma_t(t)$ traces obtained by averaging at least six spots with identical composition. The number surface density of probe, s_p, and target molecules, s_t, were obtained by dividing σ_p and σ_t by the corresponding molecular mass, respectively.

Analysis of surface hybridization by Langmuir model

The hybridization kinetics curves $\sigma_t(t)$ measured by RPI were analyzed either assuming a standard Langmuir model (11,30) or the non-Langmuir kinetic model described in Non-Langmuir Kinetic Model with Electrostatic Repulsion. The main assumptions of the Langmuir model are that the surface provides a finite number of independent binding sites (probes) holding at most one target molecule each, the binding sites are all equivalent, their properties do not change during the binding process, and there are no interactions between target molecules bound on adjacent sites. Under these assumptions, the time evolution of the fraction of hybridized surface probes $\phi(t)$ is given by

$$\frac{\partial\phi(t)}{\partial t} = k_{on}c_t(1-\phi(t)) - k_{off}\phi(t), \tag{1}$$

where c_t is the concentration of target ssDNA in solution and k_{on} and k_{off} are the kinetic rate constants for association (hybridization) and dissociation, respectively. In the experimental conditions explored in this study, the total number of immobilized probes is always much lower than the number of added targets in solution. This condition is ensured by the small size of the surface spots of probes and by a large enough sample volume. Therefore, c_t is assumed constant during the binding after each addition of sample in the measuring cartridge. Accordingly, for a concentration jump to c_t at $t = 0$, the solutions of Eq. 1 are exponential growth functions with the form

$$\phi(t) = \left(\phi_{eq}(c_t) - \phi(0)\right)\left(1 - e^{-k_{obs}t}\right) + \phi(0), \tag{2}$$

where

$$\phi_{eq}(c_t) = \frac{1}{1+\frac{K_d}{c_t}} \tag{3}$$

is the equilibrium plateau value, which depends on the dissociation equilibrium constant $K_d = k_{off}/k_{on}$ of probe-target hybridization, and

$$k_{obs}(c_t) = k_{on}c_t + k_{off} \tag{4}$$

is the observed hybridization rate. The mass surface density, $\sigma_t(t)$, or the number surface density of target, $s_t(t)$, at a given time t after an increase of concentration c_t and the asymptotic equilibrium values σ_{eq} or s_{eq} are given by $\sigma_t(t) = \phi(t)\sigma_\infty$ and $\sigma_{eq} = \phi_{eq}\sigma_\infty$ or by $s_t(t) = \phi(t)s_\infty$ and $s_{eq} = \phi_{eq}s_\infty$, respectively, where σ_∞ and s_∞ are the mass surface density and the number surface density of target at saturation reached at large c_t.

RESULTS

Effect of probe surface density on strength and kinetics of hybridization

We studied the kinetics of the hybridization process of ssDNA oligomers in solution (targets) with complementary strands (probes) immobilized on the surface of the RPI label-free biosensor. We focused on target oligomers with a length of 12 bases because they are long enough to provide rather large hybridization strengths and label-free signals and small enough to observe a clear dependence of their interaction parameters on different experimental conditions. We explored both the equilibrium constant and the kinetic rate constant for complementary probes with no additional

linker or with an ss- or ds-linker strand, as shown in Fig. 1. The injection into the RPI measuring cell of target ssDNA provides an increase of signal corresponding to the surface density of targets $\sigma_t(t)$ binding to the immobilized probes. Fig. 2 reports label-free hybridization curves measured for probes with no linker (*probe p1* in Fig. 1) after the addition of targets in solution at the concentration c_t of 100 nM. The curves correspond to different spot families on the same RPI chip produced with different probe concentrations in the spotting buffer, from 2.5 μM up to 30 μM. All curves reached a stable asymptotic value of target surface density σ_{eq} at a long time. However, both the asymptotic amplitude and the time required to reach such asymptotic value depend on the spotting concentration of probes. Like other label-free biosensors, the RPI DNA sensor enables a direct measure of the mass surface density of probes σ_p. This is derived from the brightness of the spots before the addition of target in solution, taking as reference the brightness of the region outside the spots (Supporting Materials and Methods). The number of captured target strands is roughly proportional to the number of surface probes, although it remains smaller (Fig. S1), indicating that a fraction of probe strands on the surface are not accessible to the target. In the experiment reported in Fig. 2, the hybridization yield ψ—that is, the fraction of active surface probes—was ~30%. More generally, considering all the measurements reported in this work, the obtained ψ was overall 50% $\pm$ 20%, with a tendency of copolymer coating MCP4 to provide values of ψ slightly larger than MCP2.

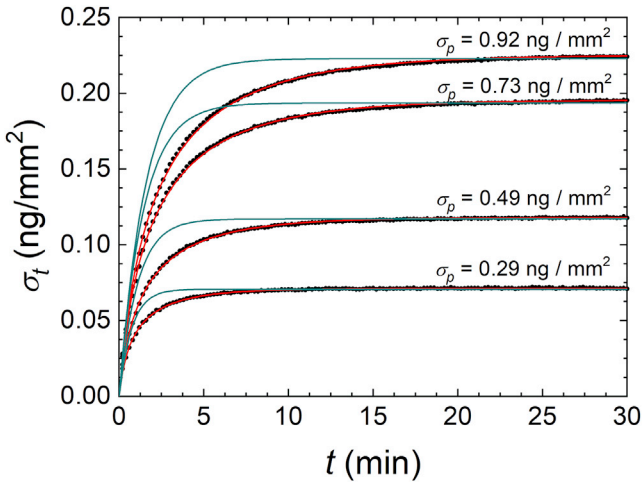

FIGURE 2 Hybridization kinetic curves measured by RPI. Binding curves (*black dots*) are expressed as mass surface density measured after the injection of 100 nM of target DNA in solution with 150 mM NaCl. The different curves refer to spots on the same RPI sensor with different surface density σ_p of DNA probes (no linker type), as reported in the figure. The DNA probes are immobilized via MCP2 copolymer. The continuous lines represent the fits with single exponential growth functions with initial slope constrained to that of the data points (*blue*) and numerical solutions of Eq. 6 (*red*). To see this figure in color, go online.

The binding curves reported in Fig. 2 also show a marked dependence of the hybridization kinetics on the surface density of probes. Smaller probe densities not only yield smaller amplitudes but also shorter times to reach the equilibrium. Under the hypothesis of an ideal interaction described by the Langmuir model, the hybridization curves should be well represented by simple exponential growth functions (Eq. 2). In contrast, the measured binding curves progressively deviates from an ideal behavior with increasing σ_p (Supporting Materials and Methods). The fit with exponential functions with constrained initial slope (*blue curves*) shows that the binding slows down after the initial stage of the hybridization curve.

This behavior suggests that the Langmuir interaction model does not represent well the hybridization kinetics between 12-mers for large surface densities of probes. Binding curves that are not well fitted by single exponentials are commonly observed by label-free biosensors and their interpretation typically involves different causes, including heterogeneity of the surface binding sites or conformational changes of probes and targets (30). A general approach is based on the assumptions of multiple Langmuir-like processes with different kinetics that sum up and yield multiexponential binding curves (31). Here, we adopted a different strategy based on a deeper investigation of the scaling of the amplitudes and rates of the binding curves progressively increasing the concentrations c_t of target in solution.

We performed sequential additions of target strands in solution, obtaining a target concentration c_t from 0.5 up to 1562.5 nM in the same RPI cell, and measured real-time hybridization curves for spot families with different spotting concentration of probes, hence obtaining a matrix of binding curves for different c_t and σ_p, as shown in Fig. 3 *a*. The inspection of the data at intermediate target concentrations (*central columns* of plots in Fig. 3 *a*) shows that the effect of σ_p on the amplitude and rates of the hybridization curves is qualitatively similar to that reported in Fig. 2. Remarkably, in this case all the measured hybridization curves are well fitted by exponential growth functions (*black curves*), even at large σ_p, because the dynamic range of each individual curve $\sigma_t(t)$ is typically smaller. This is equivalent to observing only a portion of the full curve $\sigma_t(t)$ from $\sigma_t(0) = 0$ to $\sigma_{eq}(c_t)$, such as those in Fig. 2. The fit of the measured $\sigma_t(t)$ curves with exponential functions enabled us to extract amplitudes and rates as a function of c_t and for various values of σ_p. In this way, the matrix of binding curves of Fig. 3 *a* was converted into two matrices, one for the asymptotic amplitudes $\sigma_{eq}(c_t,\sigma_p)$ and the other for the hybridization rates $k_{obs}(c_t,\sigma_p)$. The results are reported as plots at constant σ_p in Fig. 3, *b* and *c* (*blue squares*). All measured $\sigma_{eq}(c_t)$ (Fig. 3 *b*) can be approximately fitted with a simple Langmuir model according to Eq. 3 (*continuous blue curves*). The corresponding equilibrium dissociation constant K_d, indicated by the dashed lines in the figures, increases with the spotting concentration of probes,

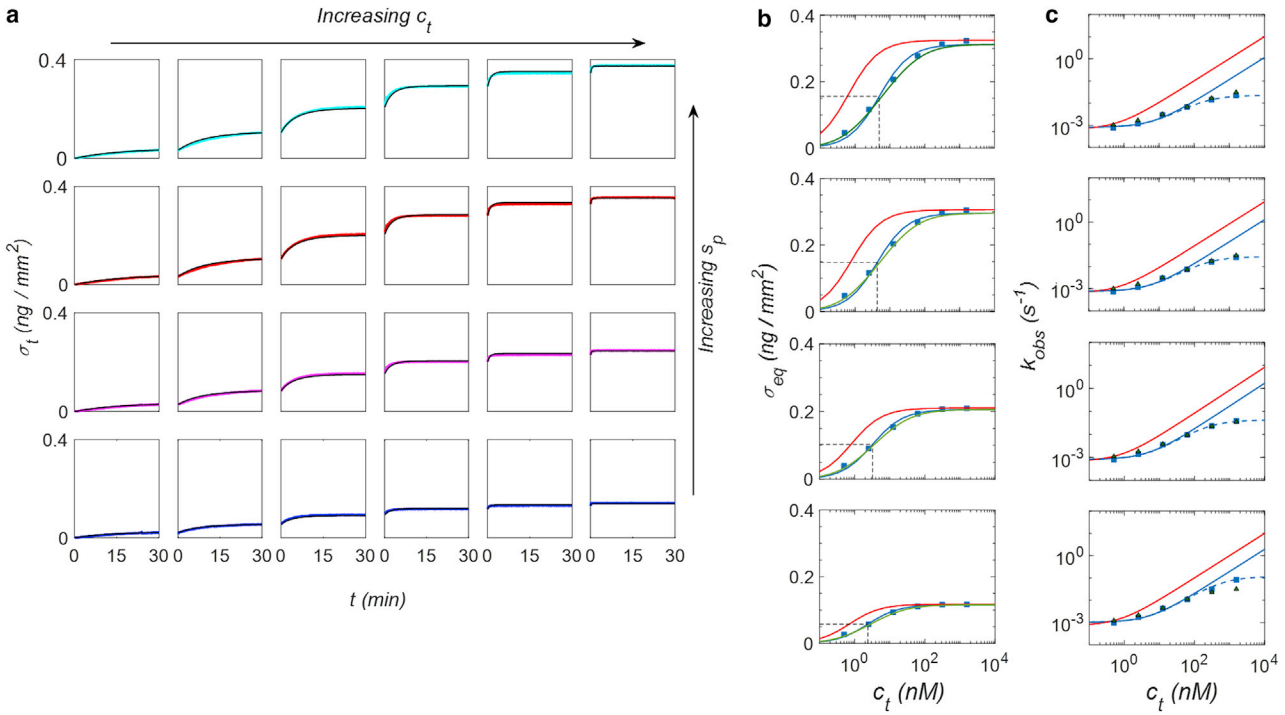

FIGURE 3 Hybridization kinetic curves at different target concentration and probe surface density. (*a*) RPI binding curves measured on the same sensor on spots with probe density 0.19 ng/mm^2 (*green*), 0.24 ng/mm^2 (*purple*), 0.38 ng/mm^2 (*red*), and 0.41 ng/mm^2 (*cyan*), for increasing concentrations of target strand in solution: (from *left* to *right*) 0.5, 2.5, 12.5, 62.5, 312.5, and 1562.5 nM. The black curves are fits to the data by single exponential growth functions. (*b*) Equilibrium asymptotic amplitudes and (*c*) kinetic rates obtained from exponential fits of the hybridization curves of panel *a* (*blue squares*). The blue lines are fits with amplitudes and rates obtained from a Langmuir model. The last two points at the largest concentrations are excluded from the fit of the rates. The green lines (*b*) and the green triangles (*c*) are the values obtained from the fit with the NLER model. The red lines represent the Langmuir behavior extrapolated from the NLER fit for $\Gamma = 0$. Average R^2-values for the equilibrium curves fits with Langmuir and NLER models reported in (*b*) are 0.987 ± 0.003 and 0.998 ± 0.001, respectively. The residual analysis is reported as Supporting Materials and Methods. To see this figure in color, go online.

suggesting a weakening of hybridization strength with the increase of σ_p. However, at a closer inspection of the amplitude data, a small systematic deviation from the ideal behavior can be observed: the fit tends to slightly underestimate the data points at concentrations c_t smaller than K_d and overestimate those for c_t larger than K_d. Residuals of the fit are reported in the Supporting Materials and Methods. For what concerns the measured hybridization rates $k_{obs}(c_t)$ (Fig. 3 *c*, *blue squares* and *continuous curve*), the analysis shows that the expected linear dependence on c_t (Eq. 4) is confirmed up to about $c_t = 100$ nM. The intercept of $k_{obs}(c_t \rightarrow 0)$, corresponding to k_{off}, appears to be constant and independent on σ_p, whereas the slope, corresponding to k_{on}, decreases with σ_p.

The observed rates clearly deviate from the ideal linear dependence on c_t only for the largest concentrations of target, when the fraction of hybridized active probes ϕ is close to 1. Fig. 3 *c* shows that the rates measured at $c_t >$ 100 nM are smaller than the values extrapolated from the dependence of $k_{obs}(c_t)$ at smaller c_t, and the deviation from the linear scaling with c_t is progressively more pronounced at increasing σ_p. We assumed that, close to saturation, the remaining small fraction of available ss probes yield to a slower association kinetics, possibly because of their close proximity to other ss probes or hybridized duplexes (32). This interpretation is consistent with the larger deviations from ideal linear scaling observed for larger σ_p and hence for smaller average probe-probe distance and is also consistent with the absence of this effect for the ds-linker probe type, in which a larger distance among neighborhood probes is maintained by the larger volume and stiffness of the ds segment. It is worth noting that the inhomogeneous probe-probe distance obtained by random immobilization of DNA strands has been also proposed as the cause of the shape of the melting curves for surface-immobilized DNA (10).

To empirically describe the observed reduction of the apparent k_{on} at large c_t, we assumed a characteristic value of the fraction of hybridized probes $\phi = \phi^*$ at which this phenomenon occurs. To estimate ϕ^*, the observed rate $k_{obs}(c_t)$ was fitted in the full range of concentrations with the following equation:

$$k_{obs}(c_t) = \frac{k_{on}C^*}{C^* + c_t}c_t + k_{off}, \tag{5}$$

where the parameter C^* represents the target concentration at which the apparent k_{on} displays a twofold decrease

relative to the low concentration value. Equation 5 well fits the data reported in Fig. 3 *c* (*dashed lines*). We converted C^* into the corresponding values of ϕ^* through Eq. 3. Fig. 4 *a* shows that ϕ^* decreases as a function of the saturation value of the number surface density of target strands s_∞ for the no linker and ss-linker hybridization types. The observed behavior is consistent with the interpretation of ϕ^* as the fraction of probe strands with a large enough distance from each other on the surface to grant free accessibility to the target strand. In each condition, an average fraction ϕ^* of probes displays a kinetics of hybridization unaffected by surface crowding. Therefore, this effect is not expected to affect the hybridization parameters for concentrations much lower than C^*.

The analysis of the amplitude and rate data of Fig. 3, *b* and *c* by a Langmuir model (Eqs. 3 and 5) enabled us to quantify the interaction parameters for the hybridization at different values of the number density of probes s_p. We obtained the kinetic rate constant for association, k_{on}, and dissociation, k_{off}, by a global fit of the amplitude and rate dependence on c_t with the constraint $K_d = k_{off}/k_{on}$. We repeated the analysis for the different probe types sketched in Fig. 1 and for the two copolymer coatings, MCP2 and MCP4. No appreciable difference was observed for the hybridization kinetics measured from the two coatings at similar s_p. However, the use of both coating types enabled us to slightly extend the overall range of s_p. As reported in Fig. 4, *b* and *c*, we found similar values of the kinetic constants for no linker and ss-linker probes and larger k_{on} and much smaller k_{off} for ds-linker. We also observed a systematic decrease of k_{on} on increasing the surface density s_p for all probe types. In contrast, k_{off} is nearly constant in the case of no linker and ss-linker probes. Therefore, the increase of K_d with s_p, reported in Fig. 4 *d*, primarily results from k_{on} in these cases. Differently, for the ds-linker probes, we obtained much smaller values of K_d and hence a stronger hybridization strength, weakly dependent on s_p. The k_{off} of the ds-linker slightly decreases with s_p, suggesting an increasing probability of rebinding of the target on the immobilized probes before diffusing away from the surface layer (33). We ascribed the peculiar behavior of the ds-linker probes primarily to the presence of the additional coaxial base stacking interaction due to the double strand adjoining the probe sequence, which can be as large as 1.5 kcal/mol in the considered experimental conditions (34,35). In contrast, the observed decrease of k_{on} with s_p reported in Fig. 4 *b* is primarily ascribed to an additional effect originating from the electrostatic repulsion between NA strands, as discussed below.

Non-Langmuir kinetic model with electrostatic repulsion

The interaction between a target ssDNA and its complementary strand immobilized on a surface is known to be affected by electrostatic repulsion (12,13,17). In particular, this effect is expected to increase with the overall surface density of NA. Consequently, the mean electrostatic repulsion in the proximity of the surface can increase during the hybridization, which brings more NAs, and hence more charges, onto the surface. This condition yields to an apparent reduction of the hybridization strength at equilibrium, which depends

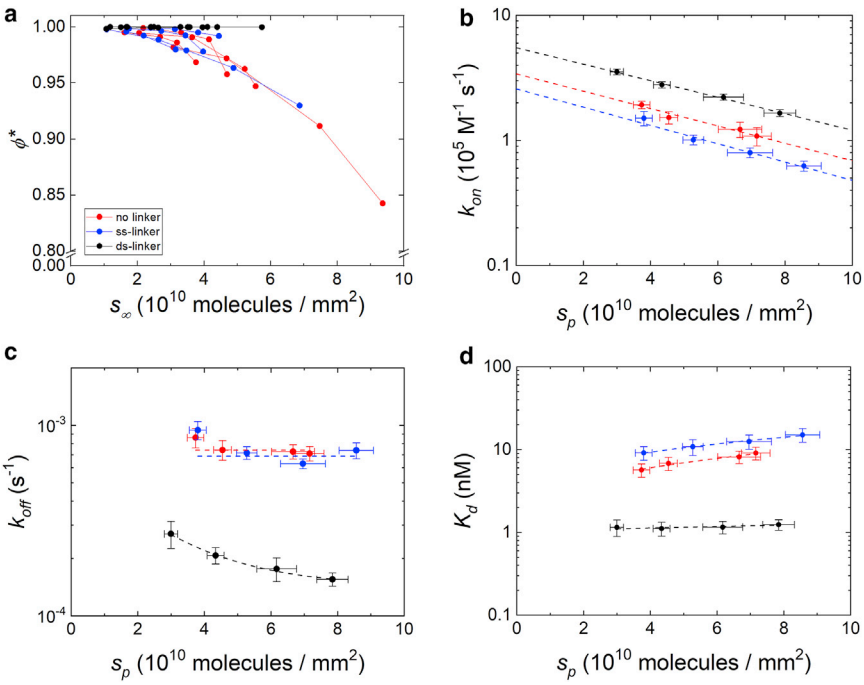

FIGURE 4 Dependence on DNA surface density of the equilibrium and kinetic parameters for hybridization. (*a*) Fraction of freely accessible probes ϕ^* as a function of target surface density s_∞ at saturation for all four experiments and all probe types. Kinetic rate for association (*b*) and dissociation (*c*) obtained for different probe types. The dashed lines represent fits to the data with the same color: constant values (*c*, *red* and *blue*) or exponential decays (all the *curves* of *b* and *black curve* in *c*). (*d*) Dissociation equilibrium constant for different probe types. The dashed lines are linear fits shown to guide the eye. In (*b*)–(*d*), the data points are average values of four experiments, and the vertical error bars are the standard deviations. Horizontal error bars are relative errors estimated from mutliple RPI experiments with the same spotting concentrations of probes. In all panels, the colors refer to different probe types, as indicated in (*a*). To see this figure in color, go online.

on the fraction of hybridized probes on the surface. Therefore, the hybridization process could show deviations from a simple Langmuir model even at small target concentrations c_t and fractional coverage of active probes ϕ. A simple theoretical solution of the equilibrium condition has been proposed by Vainrub and Pettitt (VP) (36) introducing a mean-field free-energy penalty for hybridization proportional to the surface fraction of bound active probes ϕ and accounting for an effective electrostatic repulsive potential confined in a thin surface layer. The model has been further refined by Halperin, Buhot, and Zhulina (HBZ) (37), allowing for a variable thickness of the repulsive layer and hence also describing the hybridization at low ionic strength. The notion of a repulsive potential originating at the surface of DNA biosensors and DNA arrays enables computing more accurate equilibrium solutions for the hybridization process (9,12,38). In contrast, an effective general model to account for the measured kinetics of hybridization is still missing. An influence of the surface probe density on the kinetics of DNA hybridization has been often observed in biosensor measurements (14), and a few studies have proposed theoretical frameworks accounting for electrostatic repulsion (17,32).

On the basis of the VP and HBZ equilibrium models and of the previous studies on kinetics modeling, we developed a simple approach to account for the effect of a repulsive potential in the proximity of the probe layer on the kinetics of hybridization. Fig. 5 *a* shows a schematic representation of the model: the accumulation of negative net charge on the surface yields to a repulsive electrostatic potential, which, in a simple approximation, we assume to have a step-like profile with a characteristic thickness h. At a distance larger than h from the surface, the potential is that of the bulk solution. The model also comprises the notion of a dissociation constant k_{off} substantially independent from the probe surface density, as suggested by the experiments shown in Figs. 3 and 4. Under these assumptions, the time evolution of the surface fraction of hybridized probes, for $\phi < \phi^*$, is described by

$$\frac{\partial \phi(t)}{\partial t} = k_{on}^{0} c_t e^{-\Gamma(1+n\phi)}(1-\phi) - k_{off}\phi, \qquad (6)$$

where $k_{on}{}^{0}$ is the association kinetic rate in the ideal condition of negligible repulsive interaction and Γ represents the electrostatic penalty associated with entry of charged ssDNA target into the probe surface layer, as predicted in the VP and HBZ models. The parameter n is the ratio between the length of target and probe strands expressed in number of bases and accounts for the fact that, between the conditions of $\phi = 0$ (only probe strands) and $\phi = 1$ (all active probes hybridized with the target strands), the surface charge increases by a factor $1 + n$. We named this kinetic model non-Langmuir model with electrostatic repulsion (NLER). It must be noted that the equilibrium solutions of Eq. 6 are formally identical to the surface hybridization isotherms predicted by both the VP and HBZ models and that the NLER model extends them with the treatment of kinetics. Equation 6 differs from a Langmuir kinetic model (Eq. 1) only for the exponential term $e^{-\Gamma(1\,+\,n\phi)}$, which accounts for the electrostatic repulsion experienced by the target strands in the proximity of the surface with the immobilized probes. Remarkably, this exponential term can be considered either as a correction coefficient applied to $k_{on}{}^{0}$, hence reducing the effective association time because of the repulsive free-energy barrier, or equivalently as a term applied to the concentration c_t, hence reducing the amount of target DNA effectively entering the probe surface layer. Equation 6 also indicates that the effect of the repulsive interaction yields a behavior different from a simple Langmuir process for values of the product $\Gamma \cdot n$ close to or larger than 1, a condition in which the surface density of charges changes significantly with $\phi(t)$. Considering the probe schemes shown in Fig. 1, the value of parameter n is 1 for the no linker type, 1/2 for the ss-linker, and 1/3 for the ds-linker. Notably, even if the kinetics becomes indistinguishable from a Langmuir process for small n, the repulsive interaction can still be relevant if Γ is non-negligible, and both the observed association rate

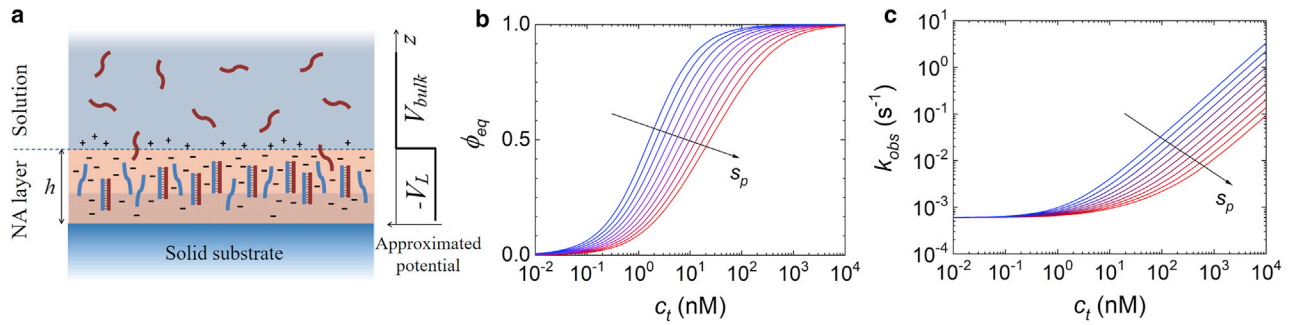

FIGURE 5 Schematic representation and numerical solution of the NLER model. (*a*) The surface region is rich in NA probes (*blue*) immobilized on the copolymer coating (*shaded area*) and hence provides a negative net charge, which further increases upon hybridization with the target strands (*dark red*). The electrostatic potential is approximated by a step function having a value lower than that of the bulk solution up to a distance h from the RPI solid surface. (*b*) Fraction of hybridized probes at equilibrium and (*c*) kinetic rate computed for different surface densities of probes, from 10^{10} mm^{-2} (*blue*) to 10^{11} mm^{-2} (*red*). The curves were computed with fixed kinetic parameters $k_{on}{}^{0} = 2.3 \times 10^{-4}$ nM^{-1} s^{-1} and $k_{off} = 7.2 \times 10^{-4}$ s^{-1} and for $\Gamma = \gamma s_p$, with $\gamma = 2 \times 10^{-11}$ mm^2. To see this figure in color, go online.

constant and the equilibrium constant effectively incorporate the term $e^{-\Gamma}$.

Numerical solutions of Eq. 6 well describe the measured hybridization curves with a minimal set of parameters. In particular, Eq. 6 describes both the nonexponential shape of the hybridization kinetic curves for large c_t jumps, as shown in Fig. 2 (*red curves*), and the dependencies of ϕ_{eq} and k_{obs} on c_t, like those reported in Fig. 3. Fig. 5 shows that $\phi_{eq}(c_t)$ and $k_{obs}(c_t)$ calculated from Eq. 6 differ from those obtained with the Langmuir model. The amplitudes $\phi_{eq}(c_t)$ of the simulated hybridization curves are shifted at larger c_t and increase with a smaller slope for larger values of Γ. Interestingly, a similar behavior can be also obtained by standard general models accounting for a distribution of interactions with different K_d or by the widely used Sips isotherm (19,39). Analogously, the observed rates $k_{obs}(c_t)$ display a progressively weaker dependence on c_t for larger values of Γ.

We used the numerical solutions of Eq. 6 to perform a two-dimensional fit of the measured hybridization curves $\sigma_t(t)$ at different c_t and s_p (Fig. 3 *a*) to extract the value of Γ, k_{on}^0, and k_{off}. The green curves in Fig. 3 *b* and the green triangles in Fig. 3 *c* report the fits to $\sigma_{eq}(c_t)$ and $k_{obs}(c_t)$, respectively. As a comparison, the red curves in Fig. 3, *b* and *c* report the amplitudes and rates extrapolated to the absence of repulsive potential at the surface, hence for $\Gamma = 0$. In this ideal condition, Eq. 6 describes a Langmuir process with kinetic rates k_{on}^0 and k_{off} and thus with $K_d^0 = k_{off}/k_{on}^0$. The behavior of both the equilibrium amplitudes and the observed rates become increasingly non-Langmuir as the surface density of probes increases. The shift at larger concentrations either for the amplitude plots (Fig. 3 *b*) or the rates (Fig. 3 *c*) provides the value of the term Γ in this process. The values of Γ are consistent with a liner scaling with s_p (Fig. S2; (37)). Therefore, we assumed

$$\Gamma = \gamma s_p, \tag{7}$$

and for each experiment, we fitted the amplitude and rate data at different c_t and s_p with only one value of k_{on}^0 and one value of γ. In the case of the no linker and ss-linker probe types, k_{off} was also assumed to be independent of s_p, whereas it was assumed to provide a linear dependence on s_p for the ds-linker probes. The average values of the kinetic parameters obtained from four experiments for each of the three probe types considered are reported in Table 2. The obtained kinetic rate constants are very similar for the no linker and the ss-linker probes and show a larger k_{on}^0 and a smaller k_{off} for the ds-linker case. The value of Γ at a standard surface density of $s_p = 10^{11}$ mm^{-2} is of the order of 1 for all probe types and shows a minimal value for the ds-linker type. Indeed, the value of Γ is expected to primarily depend on different physicochemical variables affecting the charge interactions between NAs. A deeper insight on this dependence is provided by the study of the hybridization at different ionic strengths.

Effect of ionic strength on the hybridization kinetics

The role of ionic interactions can be in general modulated by changing the solution concentration of salt, which provides the counterions that screen the chain ions. In particular, the hybridization can be partially or totally inhibited at large surface densities of probes and low concentrations of salt in solution (13). To quantitatively account for the influence of ionic strength on binding kinetics, we investigated the hybridization curves for solutions containing different salt concentration, ranging from below to above the value of ionic strength $I_s = 150$ mM, which best approximates the physiological conditions. In general, we observed an increase of the hybridization rates with I_s, and such dependence is more pronounced at low surface density of probes. Fig. 6 reports the observed hybridization rates k_{obs} as a function of s_p obtained by exponential fits of the hybridization curves $\sigma_t(t)$ measured for different ionic strengths at the same target concentration $c_t = 12.5$ nM. For all salt concentrations, the measured rates constantly decrease with s_p and tend to converge to similar values at large s_p. In the explored regimes, the values of k_{obs} span about one order of magnitude, from the smallest values measured at large probe density and small salt concentrations up to those extrapolated for small s_p and large I_s. This confirms that the hybridization kinetics can be controlled by either the surface density of probes or the salt concentration.

The observed behavior of k_{obs} as a function of surface probe density at different I_s is compatible with Eq. 6. The data reported in Fig. 6 were fitted with curves $k_{obs}(s_p)$ obtained for Eq. 6 assuming a linear dependence of k_{on}^0 as a function of I_s. Considering the range of salt concentrations explored in this study, the linear dependence of k_{on}^0 is consistent with previous measurements of kinetic rate constants for hybridization of oligomers (40,41). The obtained dependence of the characteristic value of probe density $1/\gamma$ as a function of I_s is shown in the inset of Fig. 6. The values are

TABLE 2 Measured Parameters for DNA Hybridization at 150 mM NaCl

Probe Type	Probe Sequence	Γ[a]	K_d^0 (nM)	k_{on}^0 (10^5 M^{-1} s^{-1})	k_{off}^0 (10^{-4} s^{-1})
No linker	p1	1.2 ± 0.1	2.2 ± 0.6	3.7 ± 0.7	7.7 ± 0.6
ss-Linker	p2	1.3 ± 0.3	3.0 ± 1.0	3.0 ± 1.0	6.5 ± 0.8
ds-Linker	p2 + cp2	0.8 ± 0.3	0.3 ± 0.1	6.4 ± 0.7	1.7 ± 0.5

[a]Obtained for $s_p = 10^{11}$ mm^{-2}.

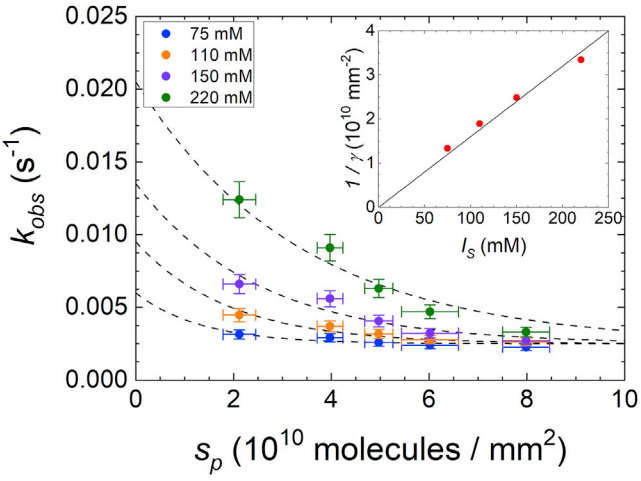

FIGURE 6 Dependence of the measured kinetic rates for hybridization on the ionic strength. RPI binding curves were measured at a target concentration of 10 nM for different surface densities of probes (no linker type) and for different ionic strength, as indicated in the figure legend. The vertical error bars represent the standard deviation of observed rates calculated from three experiments at 150 mM NaCl. Horizontal error bars are relative errors estimated from mutliple RPI experiments with the same spotting concentrations of probes. The dashed curves are fits with exponential decay functions, constrained to the same asymptotic value at large s_p and to an initial value at $s_p = 0$ linearly increasing with the ionic strength. Inset: scaling of the reciprocal of the characteristic surface γ with the ionic strength obtained from the exponential decay fit of k_{obs} (*red dots*) and linear fit with slope 16×10^{-10} $mm^{-2}M^{-1}$ (*black line*). To see this figure in color, go online.

compatible with an inverse proportionality between γ and I_s, in agreement with the expected dependence of the free-energy barrier with ionic strength. A deeper insight on the origin of the electrostatic repulsive barrier at the surface functionalized with ssDNA probe is given by the analysis of the dependence of the parameter γ on the physical features of the probe layer. According to the HBZ model, the electrostatic penalty γ takes the following form (37):

$$\gamma = 8\pi N_P N_T l_B \left(\frac{r_D^2}{h}\right), \tag{8}$$

where N_P and N_T are number of bases for probe and target strand, respectively; l_B is the Bjerrum length; r_D is the Debye length; and h is the estimated layer thickness. Given the proportionality of r_D with $I_s^{-1/2}$ (42), the value of γ is expected to scale with I_s^{-1}, in agreement with the measured values reported in Fig. 6 (*inset*).

DISCUSSION

Strength of the electrostatic repulsion

The analysis of hybridization kinetics measured by RPI confirms the relevant role of electrostatic repulsion in the observed reduction of hybridization strength on a surface. This effect is ascribed to a free-energy barrier between the free solution state and the bound state of ssDNA targets. In agreement with the VP and HBZ models, the proposed NLER kinetic model adopts a single parameter, Γ, to account for such surface repulsion effect. According to our analysis based on Eq. 6, the value of Γ can be experimentally extracted through suitably designed experiments in a range of probe and target lengths, probe surface densities, and ionic strengths in which the surface repulsion provides a modification of the hybridization kinetics relative to a simple Langmuir model. However, according to the proposed NLER model, the electrostatic free-energy barrier can be relevant even in conditions in which the surface hybridization is indistinguishable from an ideal Langmuir process, hence contributing to the observed weakening of the hybridization strength on a surface (7,19).

The quantification of the electrostatic repulsive barrier originating at the surface of a DNA biosensor has been addressed in previous works. In (37), it was shown that the data from (19), taken for a 25-mer hybridization at 1 M NaCl, are consistent with a value of $\Gamma = 3$ at $s_p = 10^{11}$ mm^{-2}, whereas a value of about $\Gamma = 11.6$ would be expected from Eq. 7 and 8. In our study, we obtained a value of $\Gamma \approx 1.2$ for 12-mer hybridization at 150 mM NaCl and $s_p = 10^{11}$ mm^{-2} (Table 2). Considering only the expected scaling of Γ with $N_P N_T$ and with I_s^{-1} (Eq. 8), which in this case roughly compensate, our values of Γ remains from 3 to 10 times smaller than those estimated in (37).

Different hybridization regimes were proposed in (13) depending on the strength of the surface repulsion: pseudo-Langmuir (PL), suppressed hybridization (SH), and no hybridization. In (17) it was estimated that for a 20-mer directly immobilized on a surface the PL-SH and the SH-no hybridization borders can be placed at $\Gamma = 2.5$ and $\Gamma = 13$, respectively. The results of our study are coherent with the conditions between an apparent Langmuir behavior at small s_p (PL) and a more complex non-Langmuir kinetics (SH), in which the repulsive barrier changes significantly during the hybridization. Therefore, a value of Γ around 2.5 would be expected. We explored a range of s_p from 2 to 15×10^{10} mm^{-2}, corresponding to a range of Γ of ~0.2–1.8 for the no linker and ss-linker probe types (Table 2), which are thus similar to the estimated threshold, although slightly smaller. A major difference between our experiments and those of (19) and (13) is that we immobilized the DNA probes on a three-dimensional (3D) copolymer coating forming a thin hydrogel layer (43), instead of a compact monolayer obtained by direct binding of DNA to the sensing surface. Therefore, from Eq. 8, the apparent discrepancy in the value of Γ can be attributed to a larger thickness h of the probe surface layer in our case.

Thickness of the surface NA layer

Because all other parameters in Eq. 8 are known or can be easily estimated, we can derive the value of the effective

thickness h of the region in which the repulsive potential is confined (Fig. 5 *a*). In the NLER model, the profile of the repulsive potential along the z coordinate perpendicular to the surface is simply approximated by a step function that remains constant within a thickness h and then decreases sharply to the bulk value of the solution. It must be noted that the actual potential will instead change gradually with the distance from the surface (17); hence, the parameter h represents the effective thickness of the step-like potential providing the same behavior of the real system. For ionic strengths around physiological conditions, the potential is expected to decrease to the bulk solution value within a few nanometers above the NA layer thickness (17,41). In contrast, if the NAs are immobilized on a 3D polymer coating, the z-profile of the repulsive potential is expected to be smoother. In the experiments performed in this study, the ssDNA probes were immobilized on the biosensor surface through a multifunctional polymeric coating capable of swelling in aqueous buffer, forming an hydrogel layer with a thickness of ~10 nm when hosting ss- or dsDNA (43). Therefore, h is expected primarily to depend on the polymer thickness h_c and on the NA layer thickness h_p as $h = h_c + h_p$. The characteristic size of the 12-mer ssDNA can be estimated assuming a persistence length of ~2.5 nm and a self-avoiding polymer scaling yielding $h_p \approx 5$ nm (44); hence, h is expected to be within 15 nm. In contrast, the value of h obtained from Eq. 8 for $N_p = N_p = 12$ is ~125 nm, hence much larger than the expected thickness of the 3D probe layer on the surface. Notably, a similar discrepancy between the measured values of Γ and those estimated by Eq. 8 was mentioned also in (37), as discussed above. Here, we propose two corrective factors to reconcile the experiments and the theoretical model. A first correction is performed considering that not all the phosphate groups of the ssDNA bring a unitary negative charge. This effect is accounted by the so-called Manning condensation (17) and yields to an effective ssDNA charge of 55% of the fully ionized molecule. Remarkably, in (17) it was reported that this charge renormalization provided the best agreement of a modified Poisson-Boltzmann model with experimental data, hence implying a complete exclusion of mobile counterions from the DNA surface layer. Because the number of charges enters Eq. 8 through the length of both probe and target DNA, this correction yields a 30% reduction of the calculated Γ for a given h. A second correction that further reduces the apparent value of Γ is obtained considering that in our experiments, not all the surface DNA probes are available for hybridization, as indicated by the yield ψ extrapolated from the saturation of the probes at large concentration of target strands. Therefore, only that fraction of probes undergoes a twofold increase of charge, whereas all the probes, not just the hybridized fraction, are responsible for the overall electrostatic repulsion at the surface. From the inspection of Eqs. 6 and 8, a constant additive term in s_p that is not multiplied by $(1 + n\phi)$ accounts for an increase of the experimentally observed value of Γ by a factor $1/\psi$, corresponding to a threefold increase for $\psi = 30\%$ as for the data in Fig. 2. Coherently, the value of h in Eq. 8 yielding such larger values of Γ is three times smaller. Together with the first correction, an overall reduction of h of about a factor of 10 is obtained, hence leading to a thickness of the copolymer layer of $h_c = h - h_p \approx 8$ nm, in agreement with previous measurements (27,43). Interestingly, this result suggests that smaller values of Γ, hence a reduction of the surface repulsion, can be theoretically obtained for much larger thickness of the 3D functional layer. However, in optical-label-free biosensors, distributing the probe molecules at constant s_p along a large thickness can yield to a decrease of signal response upon hybridization; hence, an optimal intermediate condition can be preferred.

Origin of the surface weakening of hybridization

The analysis of the hybridization at different surface probe densities enables to extrapolate the expected kinetics and equilibrium strength at very low values of s_p, when the repulsive electrostatic barrier vanishes, according to Eq. 7. In this case, the kinetic rate constant for association is given by ${k_{on}}^0$, whereas k_{off} is found to have a much weaker dependence on s_p, for the no linker and ss-linker probe types. Accordingly, the dissociation equilibrium constant at very low s_p is given by ${K_d}^0 = k_{off}/{k_{on}}^0$. Table 2 reports these values for the studied hybridization schemes. It is interesting to compare the obtained values of ${K_d}^0$ with those for both probe and target ssDNA freely diffusing in solution that can be computed by standard thermodynamic approaches (45–47). Estimates for p1-t1 and p2-t1 hybridization in solution are very similar and lie around −15 kcal/mol, corresponding to K_d of ~0.01 nM at the temperature of 23°C used in our experiments. The available algorithms do not explicitly include the stabilizing effect of coaxial stacking present in the ds-linker probe type. Nonetheless, reported values for this effect (35) can account for an additional 10-fold reduction in K_d, in line with our observations. Therefore, the estimated dissociation constant for the 12-mer hybridization in solution overall remains much lower than ${K_d}^0$ reported in Table 2. As regards kinetics, theoretical treatments are much less developed. On the basis of a set of FRET experiments (18), the predicted hybridization rate in solution for similar experimental conditions is equal to $7 \times 10^6\ \mathrm{M^{-1}\ s^{-1}}$, hence about one order of magnitude faster than what obtained for the surface probes measured in our work. Remarkably, as discussed above, a hybridization yield $\psi < 1$ suggests the presence of a constant additive term in s_p, which provides an equivalent correction factor $e^{\Gamma(1-\psi)/\psi}$ to the apparent association constant ${k_{on}}^0$ obtained from the fit of the binding curve with Eq. 6. For $\Gamma = 1.2$ and $\psi = 30\%$, this correction factor is more than one order of

magnitude, hence leading to values of $k_{on}{}^{0}$ and $K_d{}^{0}$ more similar to those estimated for hybridization in solution.

Despite the major role of electrostatic repulsion in surface hybridization, other factors can contribute to the weakening of the hybridization strength relative to the same interaction in solution. The possible sources include strand-surface interaction and interstrand interaction (9). We observed a significant non-Langmuir behavior even in the case of immobilized strands at a distance larger than their expected lateral occupancy, hence confirming that the origin of the non-Langmuir behavior is not the interstrand interaction and that the extrapolation of the hybridization strength at low s_p is not affected by possible interstrand interaction. In a previous work, we showed that a very weak interaction with the surface can induce a strong decrease of affinity for hybridization because of a simple competition effect (11). The copolymer coating used in this work is highly hydrophilic and nonionic. Therefore, electrostatic or van der Waals interactions are not expected to play a major role. However, we cannot exclude the formation of transient hydrogen bonds. Previous works have shown that immobilized DNA remains largely oriented on this copolymer coating, in agreement with the notion of negligible interactions (48).

A large effect of very weak interactions with the surface on the affinity and kinetics of hybridization is a peculiar feature of the pairing between complementary NAs, in which the binding sites are spread along the entire molecular length. The temporary unavailability of a single base of the probe strand does not prevent the hybridization but provides a strong effect on hybridization kinetics. Accordingly, on the one hand, the presence of a polymeric coating with a 3D distribution of conjugation sites can increase the thickness h and hence reduce Γ; on the other hand, it can provide more chance of weak interactions, even simply steric, with the immobilized DNA probes, hence reducing the hybridization strength with the target in solution. On the basis of these arguments, an optimal surface functionalization with DNA probes can be achieved by combining the ds-linker probe type with a conjugation layer providing suitable thickness, 3D distribution of conjugation sites, and minimal interaction with the ssDNA probe.

CONCLUSIONS

The results of this study confirm that the electrostatic repulsion is a major source of the well-known weakening of DNA hybridization on a surface in a wide range of conditions. Despite the strong effect on the equilibrium and kinetics of hybridization, a standard analysis of the binding curves can show only small deviation from an ideal Langmuir behavior. However, a two-dimensional analysis of the hybridization curves as a function of both c_t and the surface probe density s_p more easily reveals a non-Langmuir dependence coherent with a repulsive potential proportional to the overall density of NA bases on the surface, according to Eq. 6.

These results have direct consequences on the design of DNA arrays. In practice, in the explored conditions, the label-free signal due to hybridization is always found to increase with the surface density of probes. Therefore, for the purpose of assay design, larger values of s_p enable us to achieve larger signals at equilibrium for any concentration of target c_t. However, the kinetics of hybridization can be strongly reduced at large s_p by two phenomena: the surface electrostatic repulsion and the crowding of immobilized probes. The latter effect only occurs for large enough fractional coverage ϕ of probes, hence typically close to saturation, whereas the electrostatic penalty can be effective at any values of ϕ and c_t and directly contributes to reduce the observed equilibrium constant for surface hybridization. Accordingly, a correct absolute quantification of target concentration derived from the assay response should necessarily account for the weakening and slowing down of hybridization, which both depend on the surface density of probes.

Interestingly, the large net charge of NA can be considered as functional to preserve a large specificity of hybridization even at large concentrations. The electrostatic repulsion between two NA strands in solution effectively increases the threshold of the attractive strength required to form a stably paired complex, hence the minimal number of consecutive complementary bases. Indeed, uncharged DNA mimics such as peptide NAs or phosphorodiamidate morpholino oligomer, although they may provide larger affinities for hybridization with DNA in controlled conditions, also typically display the lower solubility and larger nonspecific binding that brings to relevant background signals when used in assays applications (8). Analogously, it can be argued that the enhanced repulsion originating in surface-based DNA biosensors favors the specificity of molecular recognition at the cost of sensitivity relative to DNA probes freely diffusing in solution. From the results of this study, we can estimate a DNA concentration in solution at which the electrostatic repulsion starts inducing non-negligible effects on the hybridization kinetics. From Eq. 6, we can assume that the hybridization behavior deviates from a Langmuir model for $\Gamma > 0.1$. This corresponds to s_p on the order of 10^{10} mm^{-2} for the probe srands used in this work. Considering a 3D distribution of the probes over a thickness of ~13 nm, the corresponding volume density is $\sim 8 \times 10^{17}$ molecules in 1 mL or 5 mg/mL for a 12-mer DNA probe. As a comparison, the average concentration of DNA within the nucleus is of the order of 10 mg/mL (49), with large density fluctuations in space. Therefore, the conditions achieved on the surface of DNA biosensors and the corresponding effects on hybridization can be rather common in nature and can play a biological role in the cellular nucleus.

Overall, the kinetic modeling of these elementary DNA-based interactions is expected to guide the design of more complex functional structures immobilized on a surface and provide a pathway for kinetic optimization of DNA nanomachines. The results of this work are also expected to stimulate further studies aimed at extending the modeling to a wider range of conditions, e.g., including the effect of divalent cations and DNA structures.

SUPPORTING MATERIAL

Supporting Material can be found online at https://doi.org/10.1016/j.bpj.2020.07.016.

AUTHOR CONTRIBUTIONS

L.V. designed research, analyzed data, and wrote the manuscript. T.C. and L.C. performed research. M.C. designed research. G.Z. and M.B. designed research and wrote the manuscript.

ACKNOWLEDGMENTS

This work has received funding from Regione Lombardia and FESR, Linea Accordi per la Ricerca, through the "NeOn" project (ID 239047) and from Ministero dell'Istruzione, dell'Università e della Ricerca, PRIN2017, through the "Soft Adaptive Networks" project. We thank Tommaso Bellini for useful discussions. We also thank ProXentia Srl (Milano, Italy) for providing the RPI sensing cartridges. M.B. is a founder and shareholder of ProXentia Srl.

REFERENCES

1. Bumgarner, R. 2013. Overview of DNA microarrays: types, applications, and their future. *Curr. Protoc. Mol. Biol.* Chapter 22:Unit 22.1.
2. Seeman, N. C., and H. F. Sleiman. 2018. DNA nanotechnology: from the pub to information-based chemistry. *Methods Mol. Biol.* 1811:1–9.
3. Relógio, A., C. Schwager, …, J. Valcárcel. 2002. Optimization of oligonucleotide-based DNA microarrays. *Nucleic Acids Res.* 30:e51.
4. Vasan, A. S. S., D. M. Mahadeo, …, M. Pecht. 2013. Point-of-care biosensor system. *Front. Biosci. (Schol.).* 5:39–71.
5. Zanchetta, G., R. Lanfranco, …, M. Buscaglia. 2017. Emerging applications of label-free optical biosensors. *Nanophotonics.* 6:627–645.
6. Chao, J., D. Zhu, …, C. Fan. 2016. DNA nanotechnology-enabled biosensors. *Biosens. Bioelectron.* 76:68–79.
7. Oliviero, G., S. Federici, …, P. Bergese. 2011. On the difference of equilibrium constants of DNA hybridization in bulk solution and at the solid-solution interface. *J. Mol. Recognit.* 24:182–187.
8. Qiao, W., H.-C. Chiang, …, R. Levicky. 2015. Surface vs. solution hybridization: effects of salt, temperature, and probe type. *Chem. Commun. (Camb.).* 51:17245–17248.
9. Halperin, A., A. Buhot, and E. B. Zhulina. 2006. On the hybridization isotherms of DNA microarrays: the Langmuir model and its extensions. *J. Phys. Condens. Matter.* 18:S463–S490.
10. Vainrub, A., and B. M. Pettitt. 2011. Accurate prediction of binding thermodynamics for DNA on surfaces. *J. Phys. Chem. B.* 115:13300–13303.
11. Nava, G., E. Ceccarello, …, G. Zanchetta. 2016. Label-free detection of DNA single-base mismatches using a simple reflectance-based optical technique. *Phys. Chem. Chem. Phys.* 18:13395–13402.
12. Irving, D., P. Gong, and R. Levicky. 2010. DNA surface hybridization: comparison of theory and experiment. *J. Phys. Chem. B.* 114:7631–7640.
13. Gong, P., and R. Levicky. 2008. DNA surface hybridization regimes. *Proc. Natl. Acad. Sci. USA.* 105:5301–5306.
14. Peterson, A. W., R. J. Heaton, and R. M. Georgiadis. 2001. The effect of surface probe density on DNA hybridization. *Nucleic Acids Res.* 29:5163–5168.
15. Erickson, D., D. Li, and U. J. Krull. 2003. Modeling of DNA hybridization kinetics for spatially resolved biochips. *Anal. Biochem.* 317:186–200.
16. Gao, Y., L. K. Wolf, and R. M. Georgiadis. 2006. Secondary structure effects on DNA hybridization kinetics: a solution versus surface comparison. *Nucleic Acids Res.* 34:3370–3377.
17. Wong, I. Y., and N. A. Melosh. 2010. An electrostatic model for DNA surface hybridization. *Biophys. J.* 98:2954–2963.
18. Zhang, J. X., J. Z. Fang, …, D. Y. Zhang. 2018. Predicting DNA hybridization kinetics from sequence. *Nat. Chem.* 10:91–98.
19. Peterson, A. W., L. K. Wolf, and R. M. Georgiadis. 2002. Hybridization of mismatched or partially matched DNA at surfaces. *J. Am. Chem. Soc.* 124:14601–14607.
20. Peterson, A. W., R. J. Heaton, and R. Georgiadis. 2000. Kinetic control of hybridization in surface immobilized DNA monolayer films. *J. Am. Chem. Soc.* 122:7837–7838.
21. Ouldridge, T. E., P. Šulc, …, A. A. Louis. 2013. DNA hybridization kinetics: zippering, internal displacement and sequence dependence. *Nucleic Acids Res.* 41:8886–8895.
22. Wang, R., S. Tombelli, …, M. Mascini. 2004. Immobilisation of DNA probes for the development of SPR-based sensing. *Biosens. Bioelectron.* 20:967–974.
23. Li, Z., Y. Chen, …, R. S. Williams. 2004. Sequence-specific label-free DNA sensors based on silicon nanowires. *Nano Lett.* 4:245–247.
24. Star, A., E. Tu, …, C. Valcke. 2006. Label-free detection of DNA hybridization using carbon nanotube network field-effect transistors. *Proc. Natl. Acad. Sci. USA.* 103:921–926.
25. McKendry, R., J. Zhang, …, C. Gerber. 2002. Multiple label-free biodetection and quantitative DNA-binding assays on a nanomechanical cantilever array. *Proc. Natl. Acad. Sci. USA.* 99:9783–9788.
26. Brucherseifer, M., M. Nagel, …, R. Büttner. 2000. Label-free probing of the binding state of DNA by time-domain terahertz sensing. *Appl. Phys. Lett.* 77:4049–4051.
27. Giavazzi, F., M. Salina, …, M. Buscaglia. 2013. Multispot, label-free biodetection at a phantom plastic-water interface. *Proc. Natl. Acad. Sci. USA.* 110:9350–9355.
28. Salina, M., F. Giavazzi, …, M. Buscaglia. 2015. Multi-spot, label-free immunoassay on reflectionless glass. *Biosens. Bioelectron.* 74:539–545.
29. Cretich, M., G. Pirri, …, M. Chiari. 2004. A new polymeric coating for protein microarrays. *Anal. Biochem.* 332:67–74.
30. Karlsson, R., and A. Fält. 1997. Experimental design for kinetic analysis of protein-protein interactions with surface plasmon resonance biosensors. *J. Immunol. Methods.* 200:121–133.
31. Zhao, H., I. I. Gorshkova, …, P. Schuck. 2013. A comparison of binding surfaces for SPR biosensing using an antibody-antigen system and affinity distribution analysis. *Methods.* 59:328–335.
32. Hagan, M. F., and A. K. Chakraborty. 2004. Hybridization dynamics of surface immobilized DNA. *J. Chem. Phys.* 120:4958–4968.
33. Paramanathan, T., D. Reeves, …, J. Gelles. 2014. A general mechanism for competitor-induced dissociation of molecular complexes. *Nat. Commun.* 5:5207.
34. SantaLucia, J., Jr., and D. Hicks. 2004. The thermodynamics of DNA structural motifs. *Annu. Rev. Biophys. Biomol. Struct.* 33:415–440.
35. Yakovchuk, P., E. Protozanova, and M. D. Frank-Kamenetskii. 2006. Base-stacking and base-pairing contributions into thermal stability of the DNA double helix. *Nucleic Acids Res.* 34:564–574.

36. Vainrub, A., and B. M. Pettitt. 2002. Coulomb blockage of hybridization in two-dimensional DNA arrays. *Phys. Rev. E Stat. Nonlin. Soft Matter Phys.* 66:041905.

37. Halperin, A., A. Buhot, and E. B. Zhulina. 2004. Sensitivity, specificity, and the hybridization isotherms of DNA chips. *Biophys. J.* 86:718–730.

38. Vainrub, A., and B. M. Pettitt. 2003. Sensitive quantitative nucleic acid detection using oligonucleotide microarrays. *J. Am. Chem. Soc.* 125:7798–7799.

39. Sips, R. 1948. On the structure of a catalyst surface. *J. Chem. Phys.* 16:490–495.

40. Cisse, I. I., H. Kim, and T. Ha. 2012. A rule of seven in Watson-Crick base-pairing of mismatched sequences. *Nat. Struct. Mol. Biol.* 19:623–627.

41. Dupuis, N. F., E. D. Holmstrom, and D. J. Nesbitt. 2013. Single-molecule kinetics reveal cation-promoted DNA duplex formation through ordering of single-stranded helices. *Biophys. J.* 105:756–766.

42. Atkins, P. W., and J. De Paula. 2010. Atkins' Physical chemistry. Oxford University Press, Oxford, UK.

43. Yalçin, A., F. Damin, …, M. S. Unlü. 2009. Direct observation of conformation of a polymeric coating with implications in microarray applications. *Anal. Chem.* 81:625–630.

44. Murphy, M. C., I. Rasnik, …, T. Ha. 2004. Probing single-stranded DNA conformational flexibility using fluorescence spectroscopy. *Biophys. J.* 86:2530–2537.

45. SantaLucia, J., Jr. 1998. A unified view of polymer, dumbbell, and oligonucleotide DNA nearest-neighbor thermodynamics. *Proc. Natl. Acad. Sci. USA.* 95:1460–1465.

46. Zadeh, J. N., C. D. Steenberg, …, N. A. Pierce. 2011. NUPACK: analysis and design of nucleic acid systems. *J. Comput. Chem.* 32:170–173.

47. Markham, N. R., and M. Zuker. 2005. DINAMelt web server for nucleic acid melting prediction. *Nucleic Acids Res.* 33:W577–W581.

48. Zhang, X., G. G. Daaboul, …, M. S. Ünlü. 2016. Quantitative characterization of conformational-specific protein-DNA binding using a dual-spectral interferometric imaging biosensor. *Nanoscale.* 8:5587–5598.

49. Sprague, B. L., F. Müller, …, J. G. McNally. 2006. Analysis of binding at a single spatially localized cluster of binding sites by fluorescence recovery after photobleaching. *Biophys. J.* 91:1169–1191.

Biophysical Journal, Volume *119*

Supplemental Information

Non-Langmuir Kinetics of DNA Surface Hybridization

Luka Vanjur, Thomas Carzaniga, Luca Casiraghi, Marcella Chiari, Giuliano Zanchetta, and Marco Buscaglia

1. Conversion of reflected intensity into surface density of molecules

The apparatus and the analysis algorithm of the RPI method was described in (1). Briefly, the spotted surface of the glass sensor was illuminated by collimated LED light at 450 nm and sequences of images of the reflected light were acquired by a CCD camera. The conversion of the brightness of the RPI image pixels of the spot region, u_s, and outside the spots, u_0, into surface density was performed according to:

$$\sigma(t) = \sigma^* \sqrt{\frac{u_s(t)}{u_0} - 1} - \delta\sigma \quad (1)$$

where σ^*, u_0 and $\delta\sigma$ are obtained according to (1) from the physical parameters of the RPI sensor and the refractive index of the solution.

2. Amount of hybridized DNA target strands at equilibrium

Single strand DNA oligomers with a length of 12 bases (probe type p1 in Table 1 and Figure 1) were immobilized on the surface of a RPI label-free sensor. The injection into the RPI measuring cell of complementary target ssDNA provided an increase of the measured surface density of molecules due to hybridization of the surface probes with the targets. The real-time hybridization curves were acquired from spots with different number surface density of probes s_p, after the addition of targets in solution at the concentration c_t =100 nM. The measured curves are reported in Figure 2. All curves reached a stable asymptotic value of target mass surface density σ_{eq} at long time. The asymptotic amplitude of each curve, converted from σ_{eq} into the number surface density of target at equilibrium s_{eq}, is reported in Figure S1 as a function of s_p. The number of captured target strands was roughly proportional to the number of surface probes. The hybridization yield ψ, that is the fraction of surface probes hybridized with the target, was about 30%, indicating that a fraction of probe strands on the surface were not accessible to the target.

In the framework of the NLER kinetic model described by Eq. 6, the asymptotic amplitude reached at saturation of the probe sites, i.e. at large c_t, remains proportional to the surface density of probes. However, increasing the surface density of probes, the apparent equilibrium constant for dissociation also increases (see Figure 5b), hence the saturation is reached at larger values of c_t. Accordingly, at constant c_t, the observed asymptotic amplitude deviates from a linear scaling with s_p, as shown by the dashed line in Figure S1, obtained from the numerical solutions of Eq. 6.

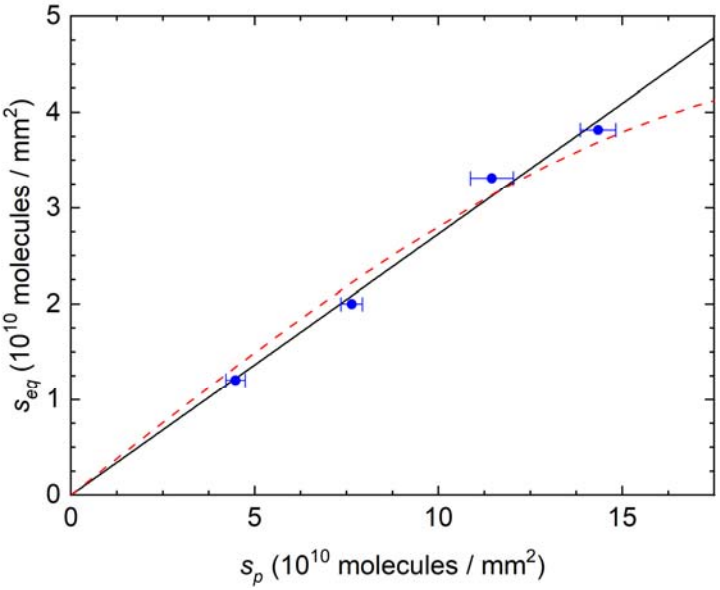

Figure S1. Scaling of hybridization equilibrium amplitude with surface probe density. The blue dots represent the equilibrium amount of DNA target strands measured from spots with different surface density s_p of probes (no linker type). The corresponding binding curves are reported in Figure 2. The black line is a linear fit with slope 0.27. The dashed line is the dependence computed from the numerical solution of Eq. 6 with $\Gamma = 0.9$.

3. Fit of the hybridization kinetic curves with free exponential growth functions

The increase of surface density of targets $\sigma_t(t)$ binding to the immobilized probes can show a non-ideal behaviour at large surface density of probes σ_p. Figure S2 reports $\sigma_t(t)$ measured for probes with no linker (probe p1) after the addition of targets in solution at the concentration c_t of 100 nM. Under the hypothesis of an ideal interaction described by the Langmuir model, we fitted the hybridization curves with simple exponential growth functions without constraints (Eq. 2). As shown in Figure S2, only the binding curve corresponding to the spots with the smallest σ_p was rather well fitted by an exponential growth (blue curves), and the deviation progressively increases with increasing σ_p. This behaviour suggests that the Langmuir interaction model does not represent well the hybridization kinetics between 12mers for large surface densities of probes.

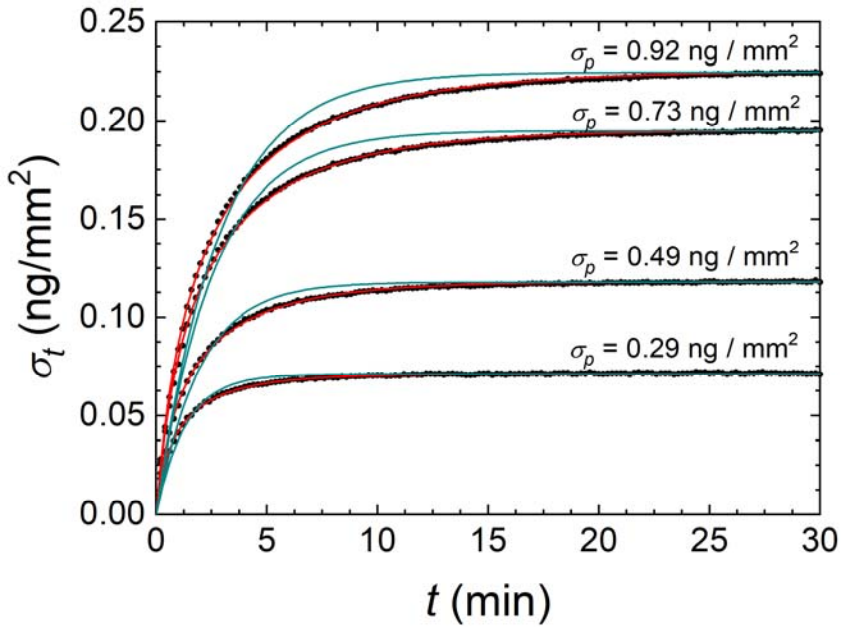

Figure S2. Free exponential fit of the hybridization kinetic curves measured by RPI. The black dots and the red curves are mass surface density data and NLER model fits shown in Figure 2 of the main text, respectively. The binding curves refer to spots on the same RPI sensor with different surface density σ_p of DNA probes (no linker type) and are measured after the injection of 100 nM of target DNA in solution with 150 mM NaCl. The light blue curves represent the best fits with single exponential growth functions without constraint.

4. Increase of electrostatic repulsion with probe surface density

Coherently with previous models describing the equilibrium behaviour of DNA surface hybridization (2)(3), the NLER kinetic model also accounts for an electrostatic repulsion increasing with the surface density of probes. The hybridization process becomes progressively non-Langmuir as the surface density of probes increases. This behaviour is accounted for by the parameter Γ in Eq. 6. If large enough, the value of Γ can be estimated from the dependence of the amplitudes and rates of the hybridization curves with c_t at constant probe density s_p. Figure S3 shows the values of Γ extracted from the fit of the hybridization curves measured for the no linker probe type, which is the case with larger n and hence larger observable deviations from a Langmuir model. The values of Γ are consistent with a liner scaling with s_p, as $\Gamma = \gamma s_p$ (Eq. 7). On the basis of this observation and on the analogous dependence predicted in (3), for each experiment we fitted the amplitudes and rates of the hybridization curves as a function of both c_t and s_p, assuming a linear dependence between Γ and s_p.

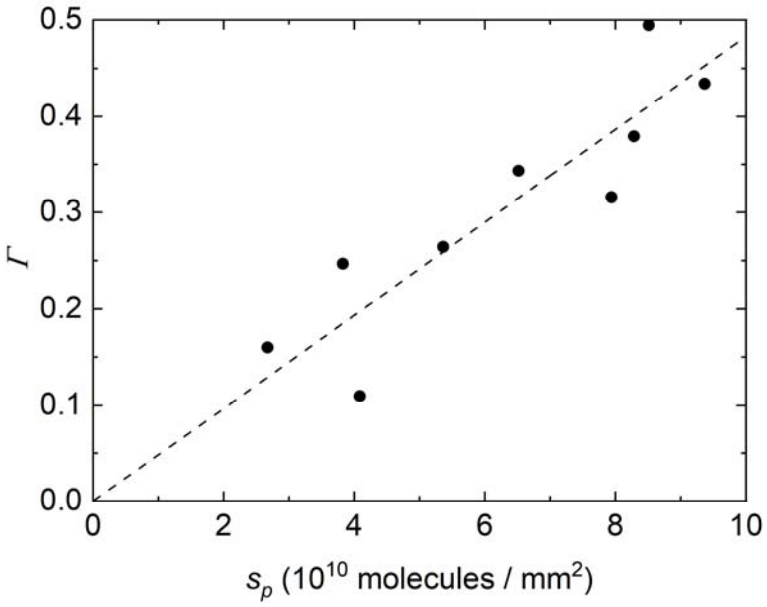

Figure S3. Measured dependence of electrostatic repulsion parameter Γ on the surface density of probes. Values of Γ obtained from the fit of the hybridization curves with the solutions of Eq. 6 for different surface density of probes (no linker type). The line is a linear fit with slope $\gamma = 0.48 \cdot 10^{-10}$ mm^2.

5. Fit quality of equilibrium curves

The equilibrium data reported in Figure 3b of the main text are better fitted by the NLER model then by the Langmuir model. In Table S1, we report the R^2 values and the residual sum of squares values (RSS) for both fits shown in Figure 3b (blue and green lines for the Langmuir and NLER model, respectively). The R^2 values for NLER model are constantly larger than those for the Langmuir model, whereas the RSS are constantly smaller. This means that the NLER model produces fits that represent the data more accurately, as also clear by visual inspection of Figure 3b. Additionally, the fit quality of the Langmuir model decreases with the increase of probe density, indicating that the DNA hybridization equilibrium data deviate more from the Langmuir model at larger probe densities. This observation is coherent with the results reported in this work.

Table S1. R^2 values and residual sum of squares (RSS) for fits to equilibrium curves in Figure 3b.

	Langmuir model		**NLER model**	
σ_p (ng/mm^2)	**R^2**	**RSS**	**R^2**	**RSS**
0.19	0.9904	$6.6 \cdot 10^{-5}$	0.9964	$2.5 \cdot 10^{-5}$
0.24	0.9887	$2.8 \cdot 10^{-4}$	0.9986	$3.3 \cdot 10^{-5}$
0.38	0.9853	$8.1 \cdot 10^{-4}$	0.9989	$6.2 \cdot 10^{-5}$
0.41	0.9836	$1.0 \cdot 10^{-3}$	0.9993	$4.5 \cdot 10^{-5}$

The residual analysis of fits in Figure 3b is shown in Figure S4. Results indicate that the NLER model is both more precise and more accurate than the Langmuir model, as indicated by the vicinity of the red dots to the zero line and their reduced spread. The larger residuals at the lowest target concentrations (c_t = 0.5) is ascribed to a lower accuracy in determining the equilibrium amplitudes of the binding curves. Overall, the difference in the fit quality between the two models increases with probe density, suggesting that the Langmuir model indeed does not represent well DNA hybridization on a surface at large probe densities.

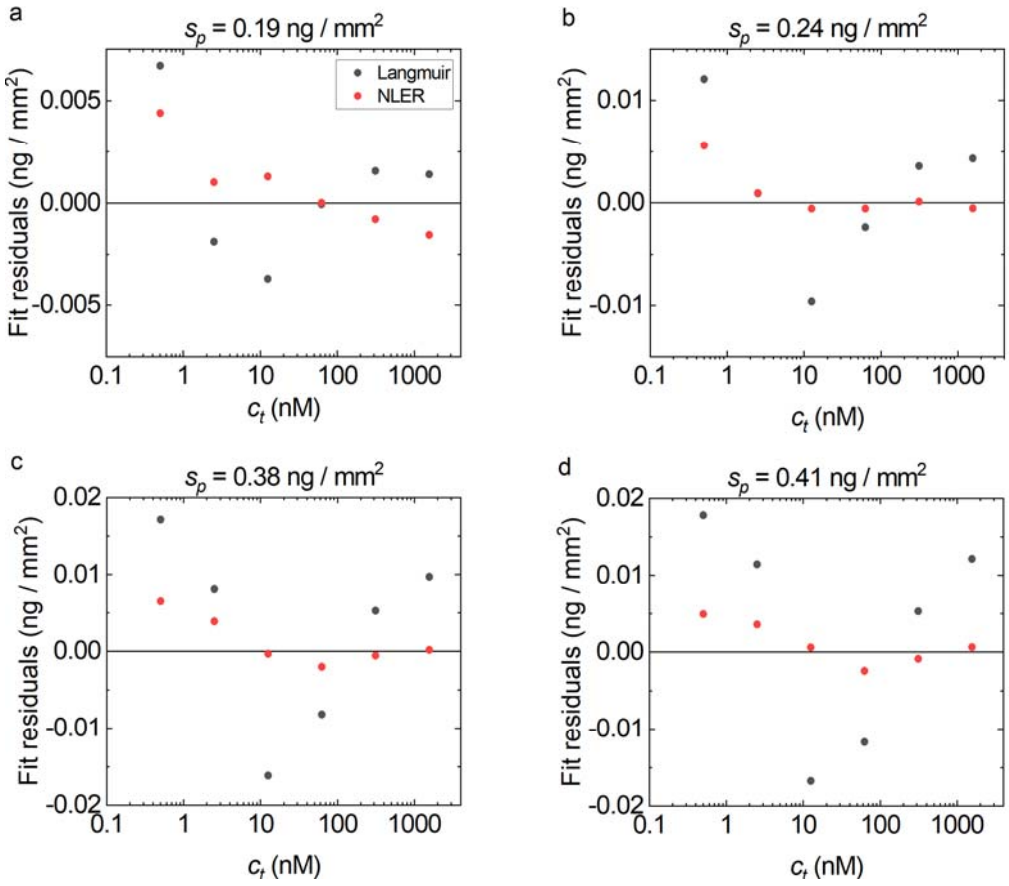

Figure S4. Fit residuals for the equilibrium data of Figure 3b. The residuals are calculated as the difference between observed value and predicted value, from the fits of both Langmuir and NLER model. NLER model fit residuals are shown as red dots, Langmuir model fit residuals are shown as grey dots. NLER model is systematically more accurate than the Langmuir model across all observed target injections, as seen in the distance from the zero line. Smaller deviation of red dots indicate that the NLER model is also more precise than its Langmuir counterpart.

References

1. Salina, M., F. Giavazzi, R. Lanfranco, E. Ceccarello, L. Sola, M. Chiari, B. Chini, R. Cerbino, T. Bellini, and M. Buscaglia. 2015. Multi-spot, label-free immunoassay on reflectionless glass. Biosens. Bioelectron. 74: 539–545.
2. Vainrub, A., and B.M. Pettitt. 2002. Coulomb blockage of hybridization in two-dimensional DNA arrays. Phys. Rev. E. 66: 041905.
3. Halperin, A., A. Buhot, and E.B. Zhulina. 2004. Sensitivity, Specificity, and the Hybridization Isotherms of DNA Chips. Biophys. J. 86: 718–730.